Identification of NEK7 Inhibitors: Structure based Virtual Screening, Molecular Docking, Density functional theory calculations and Molecular Dynamics Simulations

Mubashir Aziz
The Islamia University of Bahawalpur
Syeda Abida Ejaz (abidaejaz2010@gmail.com)
The Islamia University of Bahawalpur
Hafiz Muzzammel Rehman
University of the Punjab
M. S. Al-Buriahi
Sakarya University
Farhan Siddique
Linköping University
H. H. Somaily
King Khalid University
Z. A. Alrowaili
Jouf University

Research Article

Keywords: Molecular Docking, Density functional theory, NEK7, Simulations

Posted Date: March 21st, 2022

DOI: https://doi.org/10.21203/rs.3.rs-1445619/v1

Abstract

NEK7 plays a crucial role in many signaling pathways and contributes to a variety of cancers. Therefore, NEK7 has long been considered an attractive drug target in anti-cancer drug discovery. However, only a few efforts have been made in development of NEK7 inhibitors with selectivity. In the present study, we have investigated FDA approved kinase inhibitors as potential NEK7 inhibitors. Although more than 200 FDA approved drugs are available but none is known to inhibit NEK7 protein. These findings motivated us to design in-silico approach for investigation and identification of NEK7 protein. In the current study, Structure-based virtual screening and molecular docking were carried out to identify potential NEK7 inhibitors. Dacomitinib and Neratinib was selected depending upon their potential activities against various cancer cell lines. These drugs were subjected to density functional theory calculations which demonstrated the chemical reactivity of both drugs. Furthermore, molecular docking studies were conducted using Molecular Operating environment 2015.10 and conformations with high docking scores and strong interactions were selected for further analysis. Absorption, distribution, metabolism, elimination and toxicity (ADMET) profile evaluation was also carried out to ascertain toxicity profile of both drugs. The proposed inhibitor–protein complexes were further subjected to Molecular Dynamics (MD) Simulations studies involving root-mean-square deviation and root-mean-square fluctuation to explore the binding mode stability inside active pockets. Finally, both drugs were obtained as potential inhibitors of NEK7 protein. All these analyses provide a reference for the further development of NEk7 inhibitors.

Introduction

Cancer is uncontrolled division of abnormal cells. These cells proliferate and damage adjacent cells and organs causing metastasis [1]. A 2008 study showed cancer prevalence around 28.8 million worldwide [2]. According to World Health Organization (WHO), cancer is the second biggest reason of mortality in the world causing 10 million deaths annually [3]. Every one out of six deaths are due to cancer worldwide [4]. Kinases are proteins that are involved in normal cell regulation and cell signaling pathways [5]. Out of 497 protein kinases in human genome, 284 have been determined experimentally in apo form or inhibitor form [6]. The mutation in protein kinases disrupts its genetic makeup and can cause cell dysregulation which results in abnormal cells growth which is the main checkpoint of cancer [7]. Other factors that can cause cancer include: age, gender, lifestyle, dietary changes or exposure to toxins [8]. The example of kinases include Polo-like kinases (PLKs), cyclin-dependent kinases (CDKs), Aurora, and the Never in Mitosis (NEK) family of kinases [9]. These protein kinases are involved in cell cycle regulation [10]. Therefore, protein kinase inhibitors play an important role in cancer treatment [11]. The NEK kinase family plays a vital part in maintaining the signaling pathway of metabolic cells [12]. NEK consists of 11 proteins [13] out of which NEK6, NEK7 play an important role in cell cycle control, division and proliferation [14], and Both of these proteins have a sequence identity of 85 percent [15] NEK7 belongs to the class of NIMA related kinases [16]. NEK7 plays the most important role in mitosis compared to NEK6 or NEK9 [17]. Established studies have shown that NEK7 is involved in a number of mitotic processes like spindle assembly, placement of centrosomes, and cell division. High-throughput transcriptome study revealed that NEK7 is abundantly present in the major number of tissues like heart, liver, lung, brain, muscle, testis, leukocyte, and spleen [18] where it regulates mitotic progression [10]. Phosphorylation of a protein substrate causes it to become more active or increase its interaction with other molecules, which results in a lot of physiological responses [19]. NEK7 phosphorylates the Kinesin 5 protein (Eg5) at SER 1033, causing centrosome separation before nuclear envelop collapse [20]. Interference with NEK7 can cause unregulated phosphorylation which leads to increase in mitotic cells and ultimately leads to cell death [21]. Protein kinases have been widely studied past 20 years for the development of targets [22] to produce newer anti-neoplastic drugs [23]. 53 FDA-approved medications in the United States that have known anti-cancer action, and over 200 leads are in research for development into newer anti-cancer agents [24], but very few FDA approved inhibitors are effective against NIMA related kinases. Debrafinib is the only drug that is known to have inhibitory activity on BRAF-mutant melanoma and NRAS-mutant melanoma cell lines. These proteins were in charge of mutant melanomas' proliferation and survival. Dabrafenib, in particular, had considerable activity against NEK7 protein with an IC50 value of 1–9 nM [25]. However, none of the FDA approved drugs have inhibitory activity against NEK7 showing the scarcity of NEK7 inhibitors.

We utilized structure based in-silico approach to produce selective NEK7 inhibitors which can be used as a powerful tool for cancer therapy. Overall, docking programs show a success rate of 65–70% [26], which means that using docking programs combined or separately shows protein-ligand interaction. To enhance the accuracy of docking algorithms, the current work utilized and the commercially available Molecular Operating Environment (MOE) 2015 [27]. Additionally, the results were confirmed using comprehensive quantum chemistry calculations, including density functional theory (DFT) calculations of frontier molecular orbitals (FMOs), global and local reactivity descriptors, and molecular electrostatic potential (MEP). To determine the drug likeness and physicochemical features of compounds, detailed drug like properties, i.e. ADMET properties, were calculated. This is the first complete in -silico approach to advise future molecular exploration of these derivatives in order to identify an optimal candidate for therapeutic intervention in breast cancer and other linked malignancies.

Methods And Methodology

Computational Studies

Quantum Chemistry through Density Functional Theory Calculation

The Gaussian 09 software was used for calculation of density functional theory studies of FDA drugs and Gauss view 6 program was used for visualization of the results. The geometries of drugs were optimized using DFT/B3LYP level of theory and SVP basis set. The SVP set is reliable set for the geometry optimization of similar structures [28]. Furthermore, highest occupied molecular orbital and lowest unoccupied molecular orbital analysis was carried out using same level of theory [29].

Molecular Docking Studies

The targeted protein structure was retrieved from protein data bank [30] (PDB ID = 2wqn). The unwanted molecules such as water and unnecessary het atoms were removed from the structure using sequence editor utility of the Molecular operating environment 2015.10. Protein structure was 3D protonated and energy was minimized to steepest gradient to remove any steric clashes. Furthermore, polar hydrogen atoms and gastier charges were added using MMFF94x forcefiled. After the structure preparation, the site finder utility of the MOE was used for identification of active site of the protein. The structures of FDA approved drugs were generated using chemdraw ultra from IUPAC names. These drugs were docked into active pocket of protein using two scoring functions. The triangular matcher scoring function was set to London dg whereas placement and refinement parameters were set to GBVI-WSA dG. The rigid receptor model was used for docking purpose. After completion of Molecular docking, we selected top poses on the basis of Gibbs free binding energy, binding affinity (ki) and RMSD of the protein-ligand complex. Best poses were further analyzed and visualized using the MOE [31].

Molecular Dynamics Simulation

Molecular docking experiment provide initial protein-ligand complex for molecular dynamic studies. Desmond, a package from Schrödinger LLC [32], was used to run molecular dynamic simulation for 100 ns. Molecular docking studies provide insight into binding state of ligand with protein. Docking provides a static view of a molecule's binding pose in a protein's active site [33], MD simulations measure the average displacement of atoms with respect to some reference. MD simulation predict the stability of the protein-ligand complex [34, 35].

Maestro or protein preparation wizard was employed for processing of protein-ligand complex. The system was prepared in system builder tool. The system was solvated by PIP3P solvent model. The system was neutralized by adding counter charge particularly NACL at concentration of 0.15 M. In the simulation, the OPLS 2005 force field was used [36]. The system was equilibrated in NVT and NPT ensemble for 1 ns at 300 k temperature and 1 atm pressure. Before the simulation, the models

were loosened. After every 100 ps, the trajectories were saved for analysis, and the simulation's stability was determined by measuring the root mean square deviation (RMSD), root mean square flactuation of the protein and ligand over time [37].

Results And Discussion

Density Functional theory studies (DFTs)

In current study, Quantum chemical calculations i.e., Molecular geometry optimizations, HOMO-LUMO, Molecular electrostatic potential, frontier molecular orbital energies, energetic parameters and global reactivity descriptors of Dacomitinib and Neratinib were carried out with Gaussian 09 and Gauss view 6 software package using DFT/B3LYP method. The SVP basis set was used for all calculations [38]

Optimized geometries

In present study, geometries of FDA approved drugs Dacomitinib and Neratinib were completely optimized in gas and solvent phase using DFT/B3LYP method and 6-31g (d,p) basis set.. No negative frequencies were obtained after the geometry optimization which demonstrating that current geometries are true local minima. Optimized structures of both drugs are presented in **Figure 1.**

Table 1. Optimization energy of FDA approved drugs

Code	Gas			Methanol		
	Optimization Energy (hatree)	Polarizability a.u (α)	Dipole Moment (debye)	Optimization Energy (hatree)	Polarizability a.u (α)	Dipole Moment (debye)
Dacomitinib	-1912.731301	326.801422	2.696072	-1912.748676	435.057775	3.885410
Neratinib	-2173.707581	419.348279	6.749889	-2173.728460	560.189099	8.520631

Frontier molecular orbital analysis (FMOs)

The highest occupied molecular orbitals (HOMO) and lowest unoccupied molecular orbitals (LUMO) were generated using Gaussian 9 and Gauss view 6 software package. The energy calculations were performed using SVP basis set in gas and solvent phase. The FMOs of both drugs are shown in **figure 2.**

FMOs have high significance as they determine the reactivity of the compound. The outermost electrons are directly involve in interaction between ligand and target protein so calculation of FMOs become inevitable. The HOMO represents the ability of a compound to donate electrons while LUMO is the ability to accept or withdraw electrons. The small energy gap ΔE (E_{HOMO}-E_{LUMO}) between HOMO and LUMO represents efficient charge transfer and making molecule more polarizable. Whereas, molecules having large ΔE gap (E_{HOMO}-E_{LUMO}) are least reactive and non-polarizable [39].

The calculated values for HOMO and LUMO and ΔE gaps (E_{HOMO}-E_{LUMO}) are tabulated in **table 2.**

Table 2. Values for HOMO and LUMO and ΔE gaps (EHOMO-ELUMO)

Compound		E_{HOMO} (eV)	E_{LUMO} (eV)	ΔE_{gap} (eV)	Potential Ionization I(eV)	Affinity A(eV)	Electron donating power (ω-)	Electron accepting Power (ω+)	Electrophilicity (Δω±)
Dacomitinib	Gas	-0.21996	-0.06775	0.152	0.21996	0.06775	0.217	0.074	0.291
	Sol	-0.22054	-0.04304	0.178	0.22054	0.04304	0.217	0.074	0.291
Neratinib	Gas	-0.22254	-0.07332	0.149	0.22254	0.07332	0.230	0.082	0.312
	Sol	-0.21939	-0.07378	0.146	0.21939	0.07378	0.230	0.082	0.312

As shown in **table 2** and **figure 2**, the energy band gap between (E_{HOMO}-E_{LUMO}) for compound Dacomitinib and Neratinib were found to be 0.152eV and 0.149eV in gas phase whereas it was 0.178eV and 0.146eV in solvent phase respectively in B3LYP/DFT SVP level of theory. It was observed that small energy gap was corresponding to more reactivity of the compound. Here we can say that docking score and binding affinities of drugs increases with decrease in the energy gap. Furthermore, chemical hardness and softness is measure of stability of molecular structure. [40] Compound having the large (E_{HOMO}-E_{LUMO}) energy gap refers to hardness of molecule whereas compound having small energy gap are usually more reactive and show high binding energies and binding affinity. Dacomitinib showed softness value of 7.40 in solvent phase whereas Neratinib showed softness value of 6.25 which demonstrate that Dacomitinib is more reactive drug than Neratinib. The Koopman's theorem was used to express ionization energy and electron affinity of both drugs [41].

I = -EHOMO

A= - ELUMO

We evaluated the following parameters by using their respective formulas: Hardness: η = 1/2(ELUMO - EHOMO); Softness: S = 1/2η; Electronegativity: χ = -1/2(ELUMO + EHOMO); Chemical potential: μ = - χ; Electrophilicity index: ω = μ/2η.

Table 3. Global reactivity descriptors for FDA approved drugs

Compound		Hardness (η)	Softness (S)	Electronegativity (X)	Chemical Potential (μ)	Electrophilicity Index (ω)
Dacomitinib	Gas	0.076	6.57	0.144	-0.144	0.136
	Sol	0.089	5.63	0.132	-0.132	0.098
Neratinib	Gas	0.075	6.70	0.148	-0.148	0.147
	Sol	0.073	6.87	0.147	-0.147	0.148

It is known that outermost electrons are involved in interaction between ligand and targeted protein so it is important to calculate electron density of highest occupied and lowest unoccupied molecular orbitals. In present study we have calculated the electron density and molecular electrostatic potential (MEP) of both drugs. The electron density of HOMO in gas phase for Dacomitinib was localized over morpholine and piperdinyl ring of Dacomitinib compound whereas electron density of LUMO are localized to carbo nitrile and benzocarbazole moiety of the compound. The electron density of HOMO and LUMO for

Dacomitinib remained nearly same for solvent phase but it was more localized toward carbonitrile ring as compared to gas phase.

Molecular Docking

In-silico molecular modelling studies were conducted using MOE 2015.10 to evaluate and investigate stable protein-ligand interactions. FDA approved inhibitors i.e., Dacomitinib and Neratinib were docked into activation loop of NEK7 (PDB ID: 2WQN). Molecular docking studies showed binding affinity and interaction model of drug/protein candidate. The binding affinities of best pose was assessed through predicted inhibitory constant (***ki***) values and docking scores obtained through molecular docking. Activation loop of NEK7 protein is consist of intact HRD and DFG motifs which must remain intact to retain the active conformation of a protein. Both approved drugs were assessed for their interactions with amino acid residues of active site. Visualization of best pose was carried out using Discovery visualizer 17.2 [42]. The FDA approved drug showed excellent docking scores and formed stable protein-ligand conformation.

The docked conformation of Drug Dacomitinib with in active pocket of NEK7 formed stable protein-ligand complex with least binding energy of-26.77 kJ/mol and ***ki*** 20.37 μM. The amino acid residues which were involved in bonding and nonbonding interactions with Dacomitinib were as follows; ARG42, GLY41, ASP115, ILE40, ILE113, ALA61, LEU111, GLU112, ALA114, VAL48, ILE95, ASP179, LYS63 and PHE168. Dacomitinib showed important molecular interactions including hydrogen bonding, carbon hydrogen bonding, alkyl, pi-alkyl and van der waal interactions. All these interactions were involved in stabilizing protein-ligand complex. Briefly, it was observed that 1-ethyl piperidine ring of Dacomitinib was forming carbon hydrogen bond with ARG42 and GLY41. The formamide ring was making pi-sigma interaction with ILE40, pi-alkyl interaction withALA61 and VAL48, it is also an unfavorable acceptor-acceptor interaction with ASP179. Moreover, dimethylformadine ring is forming hydrogen bond with ASP179. Fluorobenzene ring is making pi-cation interaction with LYS63 and alkyl interaction with VAL48. Furthermore, among non-bonding interactions Van der wall interactions were observed with following residues; ASP115, LEU113, GLU112, ILE95, PHE168.

The bonding and non-bonding interactions of drug Neratinib involved important amino acid residues of activation loop of NEK7. The amino acid residues which were involved in molecular interactions with Neratinib were as follows; LEU180, LYS63, ASP179, VAL48, ILE40, ALA61, LEU113, GLU112, ALA114, ILE95, LEU111, ARG121, ASP115, GLY117, PHE168, ASP118, ALA165, LYS163 and ASN166. Neratinib showed important molecular interactions which contributed to binding affinity and binding score of protein-ligand complex. Most important interactions were observed between piperidinyl, pyrazol and 2,4 dichloro-4-floro phenyl ring of Crizotinib. Trimethylamine ring was involved in major stabilizing interaction i.e., conventional hydrogen bonding with LYS63 and ASP179 respectively of activation loop. 5-methyl-3-methylene-N-vinyl-2,3-dihydropyridin-4-amine is involved in making pi-alkyl interaction with ALA65. Moreover, chlorobenzene ring was involved in making pi-anion interaction with ASP179, pi-alkyl interaction with ALA161 and VAL48. Pyridine ring is forming pi-cation interaction with ASP179, pi-alkyl interaction with ALA114, ALA61, ILE95 and LEU111. These interactions were majorly contributing toward increasing the binding energy. Meanwhile, ethoxyethane ring was involved in carbon-hydrogen bonding with ASP115 amino acid residue. Neratinib showed excellent binding energy of -27.78 kJ/mol courtesy of important molecular interactions. Van der Walls interaction are important hydrophobic interactions which were observed with following amino acid residues; LEU180, ILE40, LEU113, GLU112, ARG121, GLY117, PHE168 and ASN166.

Molecular Dynamic simulation

The simulation paths of Desmond were examined. MD trajectory analysis was used to calculate the root mean square deviation (RMSD), root mean square fluctuation (RMSF), and protein–ligand interactions.

The Root Mean Square Deviation (RMSD) is a metric for calculating the average change in displacement of a group of atoms in relation to a reference frame. It is calculated for each and every frame of the trajectory. Throughout the simulation, monitoring the protein's RMSD can provide insight into its structural configuration. If the simulation has equilibrated, the RMSD analysis can show if the fluctuations at the end of the simulation are around some thermal average structure. The

RMSD of a ligand is shown in the plot when the protein-ligand complex is first aligned on the reference protein backbone and then the RMSD of the ligand heavy atoms is measured. If the measured values are much larger than the protein's RMSD, the ligand has most certainly diffused away from its initial binding site.

Figure 5 depicts the evolution of RMSD values for the C-alpha atoms of NEK7 protein over time. The 2wqn-Dacomitinib complex's RMSD plot (Figure 5) shows stability of the protein ligand complex throughout simulation time which show that the complex possessed stable molecular interactions. It was observed that complex reaches stability at 5 ns and remained under 2 angstrom which is perfectly acceptable. After being equilibrated, protein RMSD values fluctuate within 2 Angstrom. After 35 ns Protein RMSD was increased to 2.1 angstrom and dropped again after 50 ns but it remained within limits and remained in equilibrium for remaining simulation time. These results show that the ligands remained securely attached to the receptor throughout the simulated time. RMSD for C-alpha atoms of NEK 7 also remained under 2 angstrom which depict the structural stability of the protein.

The protein-ligand complex showed any structural changes occurred during simulation time. Trajectory analysis of protein-ligand complex showed that RMSD values remained stable. During simulation very minute changes were occur which was insignificant. It was observed that complex was stable initially but after 30 ns it showed fluctuation and RMSD reached to 2.7 angstrom. After 50 ns, complex RMSD again dropped to 1.5 angstrom and remained stable majority of the simulated time. The average value for RMSD showed that complex remained stable without significant fluctuations. It terms of Protein RMSD, it showed slight fluctuations at end of trajectory but still average value for RMSD was perfectly acceptable.

For characterizing local changes along the protein chain, the Root Mean Square Fluctuation (RMSF) is useful. Figure 6 Peaks show sections of the protein that fluctuate the greatest during the simulation on the RMSF plot. Typically, the tails (N- and C-terminal) of proteins change more than any other portion of the protein. RMSF graph depict that amino acid residues ranging from 180 to 220 showed fluctuations in RMSF value. These residues belong to C terminal lobe. Alpha helices and beta strands, for example, are usually stiffer than the unstructured section of the protein and fluctuate less than loop portions. According to MD trajectories, the residues with greater peaks belong to loop areas or N and C-terminal zones. (Figure 7). The stability of ligand binding to the protein is shown by low RMSF values of binding site residues.

Peaks show sections of the protein that fluctuate the greatest during the simulation on the RMSF plot. Typically, the tails (N- and C-terminal) of proteins change more than any other portion of the protein. Secondary structural parts such as alpha helices and beta strands are usually more rigid than the unstructured portion of the protein and fluctuate less than loop areas. The residues with higher peaks belong to loop areas or N and C-terminal zones, as determined by MD trajectories shown in **Figure 7**. The stability of ligand binding to the protein is shown by low RMSF values of binding site residues.

Conclusion

In the current study, we have conducted the *in-silico* investigation of FDA approved drugs against NEK7 protein. FDA approved drugs Dacomitinib and Neritinib was optimized and in depth electronic and reactivity parameters were calculated using DFTs studies. Both drugs exhibited reactive potential against NEK7. Molecular docking studies were performed using MOE 2015.10. Both drugs were docked into active pocket and stable conformation was retrieved on the basis of binding energies and binding affinity (ki). Both drugs showed potent molecular interactions and exhibited excellent docking scores. Furthermore results of Molecular docking experiment was supported by molecular dynamic simulations. Trajectory analysis of RMSD for protein and protein-ligand complex showed less fluctuation and retained stable conformation through simulated time. Furthermore, ADMET properties were also calculated for in-silico verification of both drugs.

Declarations

Conflict of interest

There is no conflict of interest.

Acknowledgement

Authors acknowledge Project (RCAMS/KKU/G001/21) from the King Khalid University Research Center for Advanced Materials Science (RCAMS), Saudia Arabia.

Data availability statement

All the relevant data is included in the main manuscript. All other data will be available upon reasonable request.

References

1. Seyfried TN, Huysentruyt LC. On the origin of cancer metastasis. *Crit Rev Oncog.* **2013**;18(1-2).
2. Bray F, Ren JS, Masuyer E, Ferlay J. Global estimates of cancer prevalence for 27 sites in the adult population in 2008.*IJC*. **2013**;132(5):1133-45.
3. Shibuya K, Mathers CD, Boschi-Pinto C, Lopez AD, Murray CJ. Global and regional estimates of cancer mortality and incidence by site: II. Results for the global burden of disease 2000. BMC cancer. **2002**;2(1):1-26.
4. Prager GW, Braga S, Bystricky B, Qvortrup C, Criscitiello C, Esin E, et al. Global cancer control: responding to the growing burden, rising costs and inequalities in access. *ESMO open*. **2018**;3(2):e000285.
5. Duncan JS, Turowec JP, Vilk G, Li SS, Gloor GB, Litchfield DW. Regulation of cell proliferation and survival: convergence of protein kinases and caspases. *Biochim Biophys Acta Biomembr BBA*-Proteins and Proteomics. **2010**;1804(3):505-10.
6. Modi V, Dunbrack Jr RL. Kincore: a web resource for structural classification of protein kinases and their inhibitors.*Nucleic Acids Res.Spec. Publ.* **2022**;50(D1):D654-D64.
7. Bononi A, Agnoletto C, De Marchi E, Marchi S, Patergnani S, Bonora M, et al. Protein kinases and phosphatases in the control of cell fate. *Enzyme Res.***2011**;2011.
8. Fenech M, Bonassi S. The effect of age, gender, diet and lifestyle on DNA damage measured using micronucleus frequency in human peripheral blood lymphocytes. *Mutagenesis*. **2011**;26(1):43-9.
9. Fry AM, Bayliss R, Roig J. Mitotic regulation by NEK kinase networks.*Front. Cell Dev. Biol.* **2017**;5:102.
10. Fry AM, O'Regan L, Sabir SR, Bayliss R. Cell cycle regulation by the NEK family of protein kinases.*J.Cell Sci*. **2012**;125(19):4423-33.
11. Grant S. Therapeutic protein kinase inhibitors.*Cell.Mol. Life Sci.* **2009**;66(7):1163-77.
12. Malumbres M. Physiological relevance of cell cycle kinases.*Physiol. Rev*. **2011**.
13. Quarmby LM, Mahjoub MR. Caught Nek-ing: cilia and centrioles.*J. Cell Sci.* **2005**;118(22):5161-9.
14. O'regan L, Blot J, Fry AM. Mitotic regulation by NIMA-related kinases. *Cell division*. **2007**;2(1):1-12.
15. De Donato M, Righino B, Filippetti F, Battaglia A, Petrillo M, Pirolli D, et al. Identification and antitumor activity of a novel inhibitor of the NIMA-related kinase NEK6. *Sci. Rep*. **2018**;8(1):1-13.
16. Saloura V, Cho H-S, Kiyotani K, Alachkar H, Zuo Z, Nakakido M, et al. WHSC1 promotes oncogenesis through regulation of NIMA-related kinase-7 in squamous cell carcinoma of the head and neck. Molecular Cancer Research. **2015**;13(2):293-304.
17. de Souza EE, Meirelles GV, Godoy BrB, Perez AM, Smetana JHC, Doxsey SJ, et al. Characterization of the human NEK7 interactome suggests catalytic and regulatory properties distinct from those of NEK6. *J. Proteome Res.* **2014**;13(9):4074-90.
18. Kim S, Lee K, Rhee K. NEK7 is a centrosomal kinase critical for microtubule nucleation.*Biochem. Biophys*. **2007**;360(1):56-62.
19. Hardie DG, Scott JW, Pan DA, Hudson ER. Management of cellular energy by the AMP-activated protein kinase system. *FEBS Lett*. **2003**;546(1):113-20.

20. O'Regan L, Fry AM. The Nek6 and Nek7 protein kinases are required for robust mitotic spindle formation and cytokinesis.*Mol. Cell. Biol.* **2009**;29(14):3975-90.
21. Salem H, Rachmin I, Yissachar N, Cohen S, Amiel A, Haffner R, et al. Nek7 kinase targeting leads to early mortality, cytokinesis disturbance and polyploidy. *Oncogene*. **2010**;29(28):4046-57.
22. Canduri F, Cardoso Perez P, Caceres RA, de Azevedo WF. Protein kinases as targets for antiparasitic chemotherapy drugs.*Curr.Drug Targets*. **2007**;8(3):389-98.
23. De Falco M, De Luca A. Cell cycle as a target of antineoplastic drugs.*Curr. Pharm. Des*. **2010**;16(12):1417-26.
24. Mullard A. 2020 FDA drug approvals.*Nat. Rev. Drug Discov*. **2021**;20(2):85-91.
25. Phadke M, Remsing Rix LL, Smalley I, Bryant AT, Luo Y, Lawrence HR, et al. Dabrafenib inhibits the growth of BRAF-WT cancers through CDK16 and NEK9 inhibition.*Mol.Oncol*. **2018**;12(1):74-88.
26. Bissantz C, Folkers G, Rognan D. Protein-based virtual screening of chemical databases. 1. Evaluation of different docking/scoring combinations.*J. Med. Chem*. **2000**;43(25):4759-67.
27. Group C. Molecular Operating Environment *(MOE).* **2015.**
28. Gaussian09 RAJI, Wallingford CT. 1, mj frisch, gw trucks, hb schlegel, ge scuseria, ma robb, jr cheeseman, g. Scalmani, v. Barone, b. Mennucci, ga petersson et al., gaussian. **2009;**121:150-66.
29. Azarakhshi F, Khaleghian M, Farhadyar NJLiOC. DFT study and NBO analysis of conformational properties of 2-Substituted 2-Oxo-1, 3, 2-dioxaphosphorinanes and their dithia and diselena analogs. **2015**;12(7):516-22.
30. Morris GM, Lim-Wilby M. Molecular docking. Molecular modeling of proteins: Springer; **2008**. p. 365-82.
31. Prieto-Martínez FD, Arciniega M, Medina-Franco JLJTReecq-b. Molecular docking: current advances and challenges. **2018**;21.
32. Bowers KJaC, David E. and Xu, Huafeng and Dror, Ron O. and Eastwood, Michael P. and Gregersen, Brent A. and Klepeis, John L. and Kolossvary, Istvan and Moraes, Mark A. and Sacerdoti, Federico D. and Salmon, John K. and Shan, Yibing and Shaw, David E. Scalable Algorithms for Molecular Dynamics Simulations on Commodity Clusters: *IEEE;* **2006.** 43- p.
33. Ferreira LG, Dos Santos RN, Oliva G, Andricopulo AD. Molecular docking and structure-based drug design strategies. *Molecules*. **2015**;20(7):13384-421.
34. Hildebrand PW, Rose AS, Tiemann JKS. Bringing Molecular Dynamics Simulation Data into View. *Trends Biochem Sci*. **2019**;44(11):902-13.
35. Rasheed MA, Iqbal MN, Saddick S, Ali I, Khan FS, Kanwal S, et al. Identification of Lead Compounds against Scm (fms10) in Enterococcus faecium Using Computer Aided Drug Designing. *Life* (Basel). **2021**;11(2).
36. Shivakumar D, Williams J, Wu Y, Damm W, Shelley J, Sherman W. Prediction of Absolute Solvation Free Energies using Molecular Dynamics Free Energy Perturbation and the OPLS Force Field.*J.Chem. Theory Comput*. **2010**;6(5):1509-19.
37. Zhang Y, Zhang T-j, Tu S, Zhang Z-h, Meng F-hJM. Identification of Novel Src Inhibitors: Pharmacophore-Based Virtual Screening, Molecular Docking and Molecular Dynamics Simulations. **2020**;25(18):4094.
38. Bauernschmitt R, Häser M, Treutler O, Ahlrichs R. Calculation of excitation energies within time-dependent density functional theory using auxiliary basis set expansions. *Chem. Phys. Lett.***1997**;264(6):573-8.
39. Hossen J, Ali MA, Reza S. Theoretical investigations on the antioxidant potential of a non-phenolic compound thymoquinone: a DFT approach.*J.Mol. Model*. **2021**;27(6):1-11.
40. Thanikaivelan P, Subramanian V, Rao JR, Nair BU. Application of quantum chemical descriptor in quantitative structure activity and structure property relationship.*Chem.Phys. Lett.* **2000**;323(1-2):59-70.
41. Ehresmann B, de Groot MJ, Alex A, Clark T. New molecular descriptors based on local properties at the molecular surface and a boiling-point model derived from them. *J Chem Inform Comput Sci*.**2004**;44(2):658-68.
42. Studio D. Discovery Studio. *Accelrys* . **2008**.

Figures

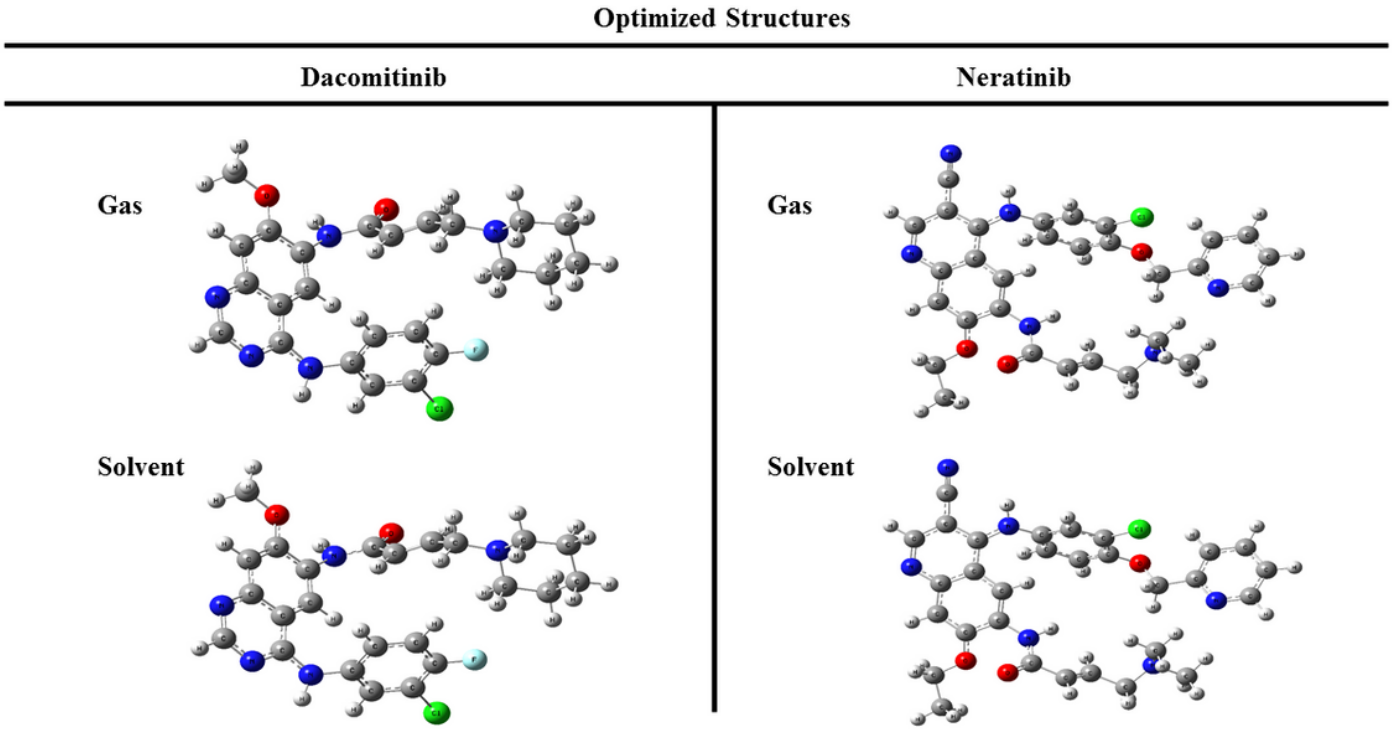

Figure 1

Optimized structures of Dacomitinib and Neritinib

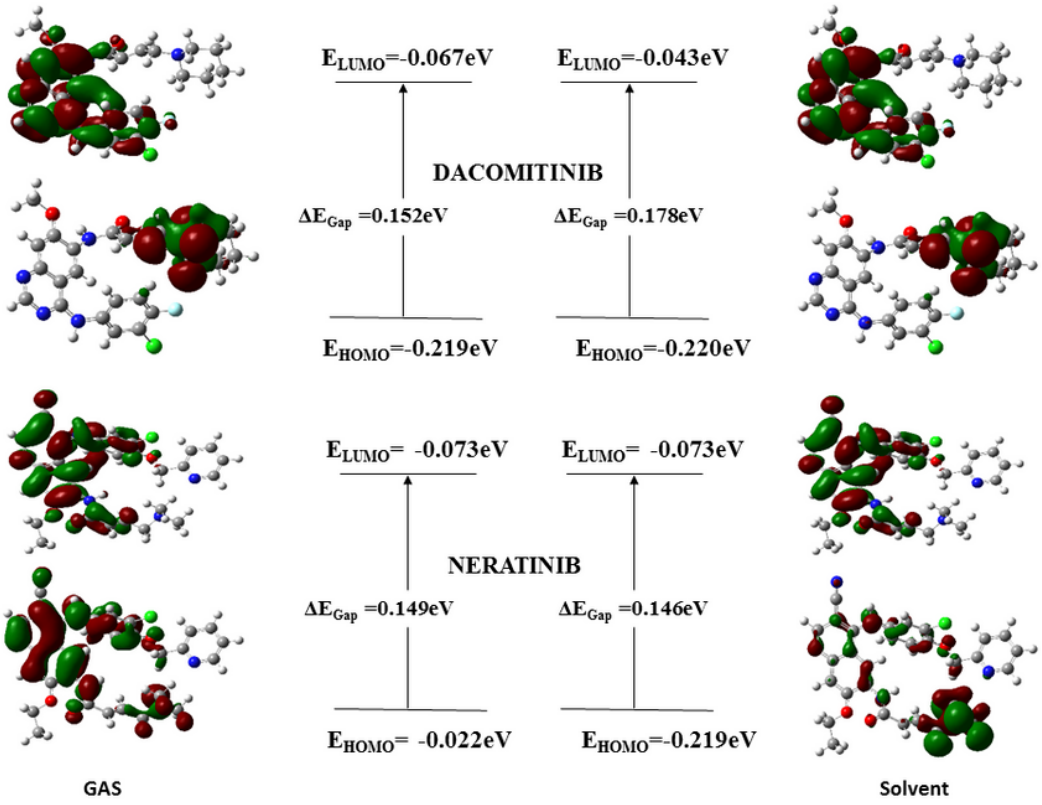

Figure 2

HOMO and LUMO in gas and solvent (water) phase

Figure 3

2D and 3D interactions for NEK7- Dacomitinib complex

Figure 4

2D and 3D interactions for NEK7- Neratinib complex

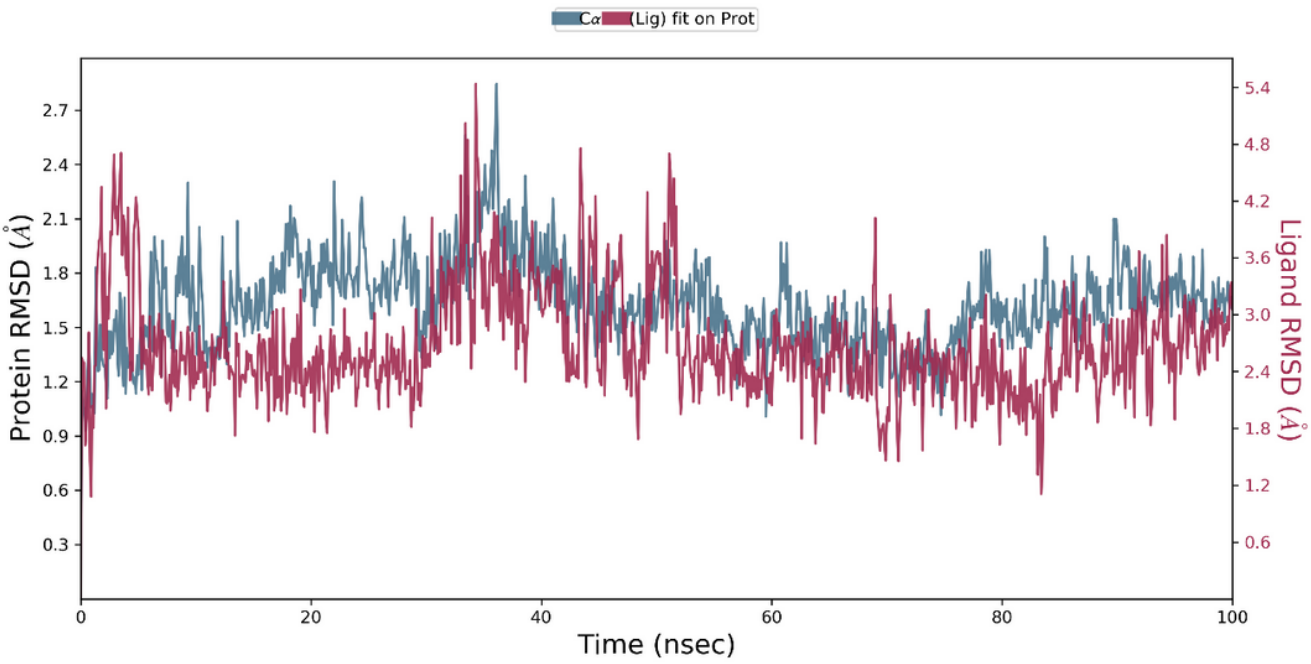

Figure 5

Residue wise Root mean square deviation (RMSD) of the C-alpha atoms of NEK7 (2wqn) and Dacomitinib Complex with time the left Y-axis depicts the change in protein RMSD over time. The right Y-axis depicts the change in ligand RMSD over time.

Figure 6

Residue wise Root mean square deviation (RMSD) of the C-alpha atoms of NEK7 (2wqn) and Neratinib Complex with time the left Y-axis depicts the change in protein RMSD over time. The right Y-axis depicts the change in ligand RMSD over time.

Figure 7

Root mean square fluctuations (RMSF) of the C-alpha atoms of NEK7 (2wqn)

Supplementary Files

This is a list of supplementary files associated with this preprint. Click to download.

- Graphicalabstract.png